STEREO PIV AND LDA MEASUREMENTS AT THE AXIAL FAN OUTLET

Đ.S. ČANTRAK[1,c], N.Z. JANKOVIĆ[1], M.S. NEDELJKOVIĆ[1], M.R. LEČIĆ[2]

[1]Hydraulic Machinery and Energy Systems Department, Faculty of Mechanical Engineering, University of Belgrade, Belgrade, 11120, Serbia

[2]Fluid Mechanics Department, Faculty of Mechanical Engineering, University of Belgrade, Belgrade, 11120, Serbia

[c]Corresponding author: Tel.: +381113302363; Fax: +381113370364; Email: djcantrak@mas.bg.ac.rs

KEYWORDS:

> **Main subjects**: Experimental fluid mechanics, flow visualization
> **Fluid:** incompressible flow
> **Visualization method(s):** particle image velocimetry
> **Other keywords:** swirl flow, turbulence, SPIV, LDA

ABSTRACT: Turbulent swirl flow in the field of hydraulic machines and systems occupies attention of many researchers in laboratories and industry, as it has significant influence on energy consumption and fan design. Physical understanding of this phenomenon would enlighten many unsolved problems and help developing new turbulent numerical models for CFD analysis. Distribution and mutual influences of the time averaged and fluctuation velocity fields to each other have been investigated in this paper. Test rig is consisted of circular pipe sections with total length 27.74·D, where D=0.4m is pipe inner diameter. Specially designed axial fan, which generates Rankine's type swirl, is positioned at the test rig inlet following profiled free-bell mouth inlet. Stereo Particle image velocimetry (SPIV) and one-component Laser Doppler Anemometry (LDA) have been conducted in the measuring section x/D=3.35 from the test rig inlet. In this paper is presented vortex core dynamics for five Reynolds numbers defined with five equally distributed fan rotation numbers in the interval n=500 till 2500rpm. Criterion of minimum total velocity has been employed. Percentage of the unique points remain almost constant for all five regimes. Distribution of the statistical moments of higher order, determined on the basis of LDA measurements, gives better understanding of the turbulent swirl velocity field. Visualization with Nd:Yag laser, max 30fps camera and paraffin oil has been performed in the cross section x/D=26.31 for better understanding of the vortex core dynamics.

NOMENCLATURE

D	$[m]$	inner pipe diameter	r	$[m]$	radial coordinate
D_i	$[m]$	hub diameter	t	$[s]$	transit time
D_a	$[m]$	impeller diameter	u	$[m/s]$	fluctuating axial velocity
F	$[-]$	flatness factor	v	$[m/s]$	fluctuating radial velocity
Q	$[m^3/s]$	volumetric flow meter	w	$[m/s]$	fluctuating circumferential velocity
N	$[-]$	number of samples	x, y	$[mm]$	fluid coordinate system
R	$[m]$	inner pipe radius	x	$[m]$	axial coordinate along a pipe axis
Re	$[-]$	Reynolds number	Γ	$[m^2/s]$	average circulation
S	$[-]$	skewness factor	Ω	$[-]$	swirl flow parameter
T	$[-]$	turbulence intensity	β_a	$[°]$	blade angle at impeller diameter
U	$[m/s]$	mean axial velocity	η	$[-]$	weighting factor
V	$[m/s]$	mean radial velocity	σ	$[m/s]$	root-mean-square of the turbulent velocity fluctuations
W	$[m/s]$	mean circumferential velocity			
c	$[m/s]$	total velocity	φ	$[°]$	coordinate of the polar cylindrical coordinate system (x,r,φ)
n	$[rpm]$	fan shaft rotational speed			

1. INTRODUCTION

Research of the turbulent swirl flow on the pressure side of axial fan, which generates Rankine's swirl, is presented in this paper. Mean and turbulent velocity characteristics of this swirl type have been investigated [1-8]. Measurements have been performed with one-component laser Doppler anemometry (LDA) system and stereoscopic particle image velocimetry (SPIV). Values of skewness and flatness factors differ from normal distribution values.

2. TEST RIG

Experimental test rig is circular pipe 27.74·D long, where D=0.4m is pipe inner diameter (Fig. 1.). It is consisted of four sections, of which two are transparent each 4m long and two transparent at the test rig inlet and outlet. SPIV and LDA measurements have been performed in the measuring cross-section x/D=3.35, where x is measured from the test rig inlet. Visualization with Nd:Yag laser, 32fps camera and paraffin oil has been performed in the cross section x/D=26.31.
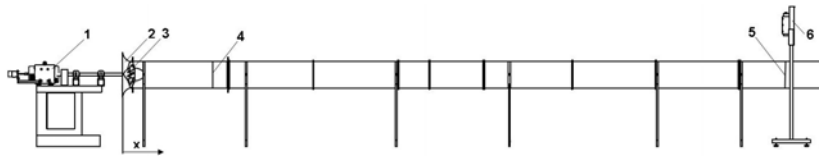
Fig. 1 Test rig: 1-DC motor, 2- profiled free bell-mouth inlet, 3-axial fan, 4-LDA and SPIV measuring section, 5-visualization section and 6-Nd:Yag laser.

Fan rotation speed was regulated by a fully automated thyristor bridge with error up to ±0.5rpm, originally designed and made by Prof. Dr.-Ing. Zoran Stojiljković. In this paper are presented results for fan rotational speed with five equally distributed fan rotation numbers in the interval n=500 till 2500rpm. Swirl generator is a variable pitch axial fan designed by Prof. Dr.-Ing. Zoran Protić[†]. This axial fan has nine blades and has been designed after rW=const. law. The impeller diameter is D_a=0.399m. Dimensionless hub ratio is D_i/D_a=0.5. The blade angle at impeller diameter was adjusted to β_a=30º. Ambient conditions have been recorded.

3. EXPERIMENTAL METHODS

3.1 LDA Measurements

LDA measurements have been performed by use of one-component LDA system along the vertical diameter in points on distance 10mm each in defined sections. It has been performed for all three components subsequently. Axial and radial velocities were measured from a side, while circumferential from above and below, because focus length was not big enough for the whole section. Overlapping of the measured points in the vortex core was obtained in this way.

LDA system was Flow Explorer Mini LDA, Dantec, with BSA F30 signal processor model. Focus is at 300mm, power 35mW, wavelength 660nm, measuring volume is approximately 0.1x0.1x1 mm and possible maximum velocity is 27m/s. Producer specified measuring uncertainty is 0.1%. It works in backscattered mode. Transit time was used as weighting factor. Recording time of 10s was set as stop criteria for all measurements. Data frequency varied along the vertical diameter depending of the measured velocity component and regime. Maximum achieved data rate is 31,76kHz for circumferential velocity. The data validation during test was in average greater than 85% for circumferential velocity. Sensitivity was adjusted in the interval 1000-1400V with step 200V. Acqustion was done in BSA software, while data processing was performed by self made programs in MatLAB. Flow was seeded by Antari Z3000II fog machine with liquid EFOG, Density Fluid, Invision. Fog was thermally generated. Enough seeding was obtained by axial fan naturally suction in the test rig.

3.2 SPIV Measurements

Stereo PIV system by TSI, USA was used in these investigations. System consisted of dual head Nd:Yag laser (max power: 30mJ/pulse, wavelength 532nm, 15Hz), two 12-bit CCD cameras (resolution 1660x1200 pixels, 32fps, lenses 50mm/F1.8), frame grabber and synchronizer with minimum frame straddling time 200ns. Mounted laser light sheet optics was spherical lens with focal length 500mm and cylindrical lenses with focal lengths -25 and -15mm.

Cameras were working in back scatter mode and positioned in Scheimpflug setup (Fig. 2.). Laser light sheet was passing between the cameras. INSIGHT 3G TSI software was used for data acquisition and processing. The post-processing was performed in Tecplot and in-house programs written in Matlab. Number of taken pictures was 400 with frequency 2Hz, as data storage was not so speed.
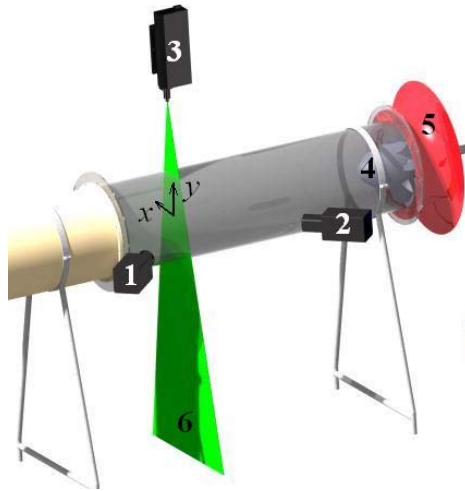
Fig. 2 SPIV setup in measuring section: 1-left camera, 2-right camera, 3-Nd:Yag laser, 4-axial fan, 5-profiled free bell-mouth inlet and 6-laser light sheet with fluid coordinate system.

Flow seeding was performed in the same way as in LDA measurements. Processing was performed with deformation grid, deformation mask, FFT correlation and Gaussian peak. Starting interrogation window was 64x64 pixels, while final 32x32 pixels [9,10]. Maximum displacement was 8. In addition, validation was performed. Any missing vectors were interpolated using a 3x3 local mean technique [11]. The percentage of interpolated vectors was for both cameras around 3%.

4. LDA EXPERIMENTAL RESULTS AND ANALYSIS

4.1 LDA

4.1.1 Integral characteristics of turbulent swirl flow

Distribution of axial, circumferential and radial velocity for all five regimes is given in Figure 3. Angle $\varphi=90º$ denotes upper part (above pipe axis) of the vertical diameter, while $\varphi=270º$ lower part (under pipe axis).
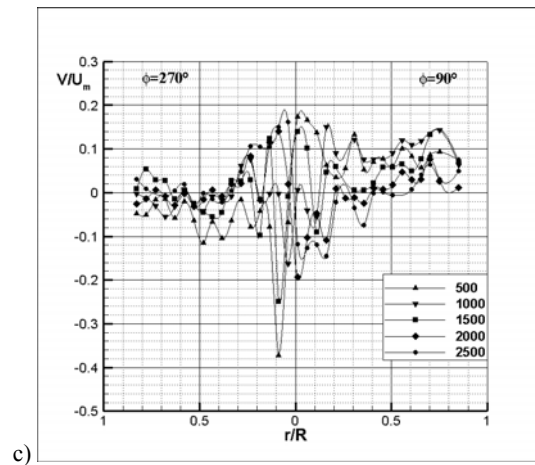
c)
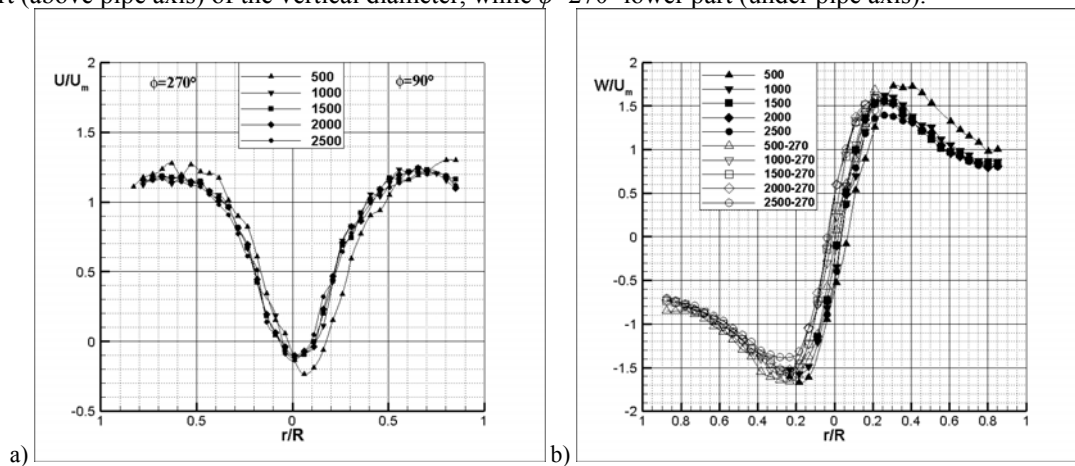
Fig. 3 Velocity distributions in measuring cross-section for all five regimes: a) axial, b) circumferential and c) radial.

It is obvious that velocity profiles are similar to each other for all five regimes. Regions of vortex core, shear layer and sound flow region are most obvious at circumferential velocity diagram (Fig. 3b). Vortex core region is in almost all the cases the same and its diameter is approximately 0.35·R. It is characterized with solid body distribution.

Reverse flow is present for all regimes (Fig. 3a). Minimum of axial and circumferential velocity is in almost the same point. Values of circumferential velocity are greater than axial. Radial velocity reaches its maximum for all regimes in a vortex core. In the sound flow region distribution law rW=const. is obvious.

Integral flow characteristics are calculated on the basis of axial and circumferential velocity distribution with estimation of axisymmetry. Volume flow rate and axial average velocity are calculated as follows:

$$Q = 2\pi R^2 \int_0^1 kU \, \mathrm{d}k, \quad U_m = \frac{Q}{R^2\pi},$$ (1)

where k=r/R is dimensionless radius. Average circulation is calculated in the following way:

$$\Gamma = \frac{4\pi^2 R^3}{Q} \int_0^1 k^2 UW \mathrm{d}k.$$ (2)

Swirl flow parameter is obtained as follows:

$$\Omega = \frac{Q}{R\Gamma}.$$ (3)

Reynolds number is calculated on the basis of averaged axial velocity Re=$U_m D/v$, where D is 0.405m in this measuring section.

Obtained values are given in the following table.

Table 1. Integral characteristics of turbulent flow.

Regime	n [rpm]	Q [m³/s]	U_m [m/s]	Re	Γ [m²/s]	Ω
1	500	0.422	3.11	85122	3.09	0.64
2	1000	0.849	6.68	182602	5.41	0.79
3	1500	1.319	10.13	277018	7.91	0.81
4	2000	1.742	13.52	369612	10.51	0.82
5	2500	2.206	17.17	469612	13.12	0.83

It is normal that average circulation across the measuring section, for the same fan, increases with Re. Swirl flow parameter has significant increases up to the third regime, where stays almost constant for the last three regimes.

4.1.2 Flow turbulent characteristics

Turbulent characteristics by introducing a non-uniform weighting factor (η_j) in order to correct velocity-bias minimize are calculated in the following way (Table 2.).

Table 2. Turbulent characteristics calculation.

Reynolds normal stresses	$$\overline{u_i^2} = \sum_{j=0}^{N-1} \eta_j \left(u_i^2\right)_j, \quad \eta_j = \frac{t_j}{\sum\limits_{k=0}^{N-1} t_k}$$
Turbulence intensity	$$T_i = \frac{\sigma_i}{U_m} = \frac{\sqrt{\overline{u_i^2}}}{U_m}$$
Skewness and flatness factors	$$S_i = \overline{u_i^3} / \sigma_i^3, \quad F_i = \overline{u_i^4} / \sigma_i^4.$$

Here t_j is transit time of the j-th particle crossing the measuring volume and $u_i=u,v,w$, $U_i=U,V,W$.

Turbulence characteristic for axial velocity are given in the following pictures.
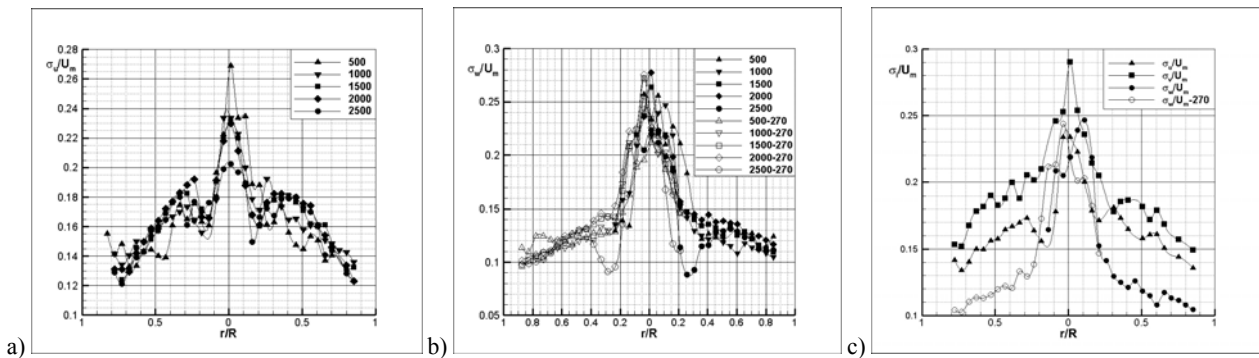
Fig. 4 Turbulence intensity for a) axial and b) circumferential velocity; c) Anisotropy for all three velocities for the second regime.

Maximum values of the turbulence intensity for axial, as well as for circumferential velocity, are reached in the vortex core region with tendency for increasing in the wall region (Fig. 4 a) and b)). Anisotropy and non-homogeneity is shown for the second regime (Fig. 4c). Turbulence intensity is the highest for radial and lowest for circumferential velocity. Distribution for velocity components is almost axis-symmetrical.
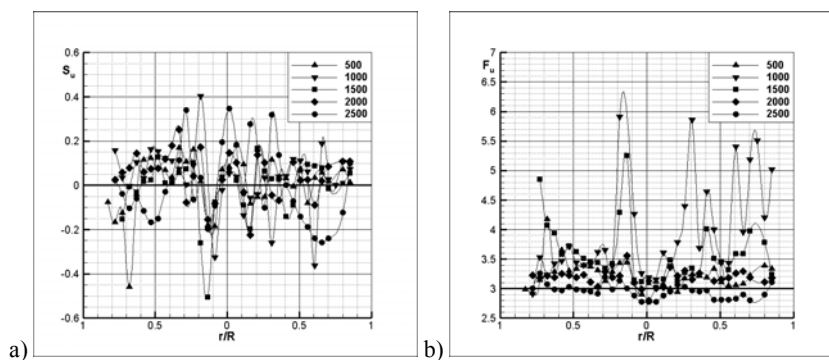

Fig. 5 a) Skewness and b) flatness factors axial velocity for all five regimes.

Values of the normalized central moments for axial velocity of the third S_u (skewness) and the fourth order F_u (flatness) are given in the previous diagrams. It is obvious that skewness and flatness factors for all regimes differ from values for normal distribution ($S_i=0$ and $F_i=0$), what was also shown in [6.7]. This is the same case for radial and circumferential velocity. Negative skewness factors, present in each regime, indicate that large velocity fluctuations are negative. Values of flatness factors greater than value 3 indicate great probability of small fluctuations. This is a case in almost all regimes, but in very few points for the fifth regime. Maximums are reached for the first two regimes, especially the second one. This is not the case for circumferential velocity.

4.2 Stereo PIV

4.2.1 Time averaged velocity distributions

Measurements have been performed in cross-section, with target size approximately 180x90mm. Target origin is on the pipe axis (Fig. 2). Velocity vectors and their intensities are given in Fig. 6. These results are obtained on the basis of averaging 400 pictures taken with 2Hz.
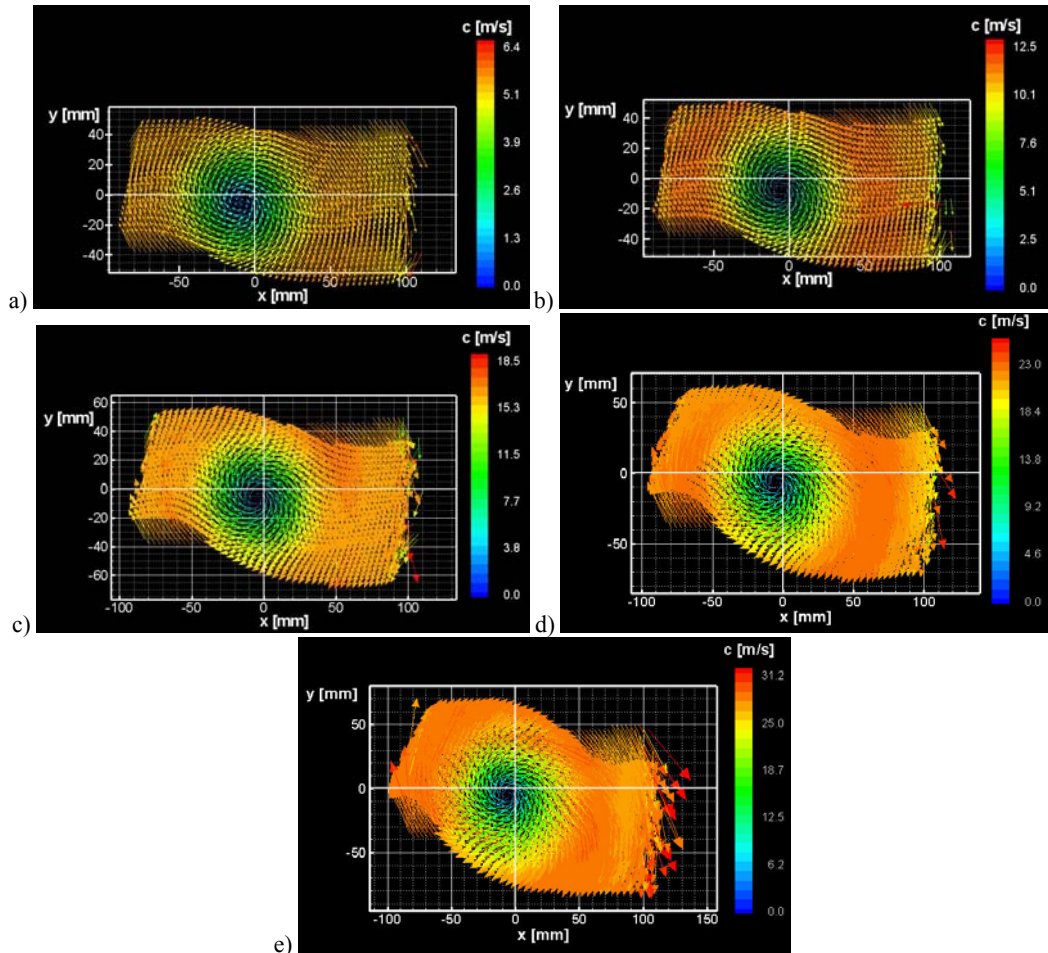

Fig. 6 Total velocity vectors and intensities for all five regime from 500 till 2500 rpm respectively.

It can be seen that vortex center, defined as the total velocity minimum is off axis. It is, for all five regimes, in the third quadrant. This will be shown later. Velocity components have been recalculated to the polar-cylindrical coordinate system and presented in the Fig. 7 only for the third regime.
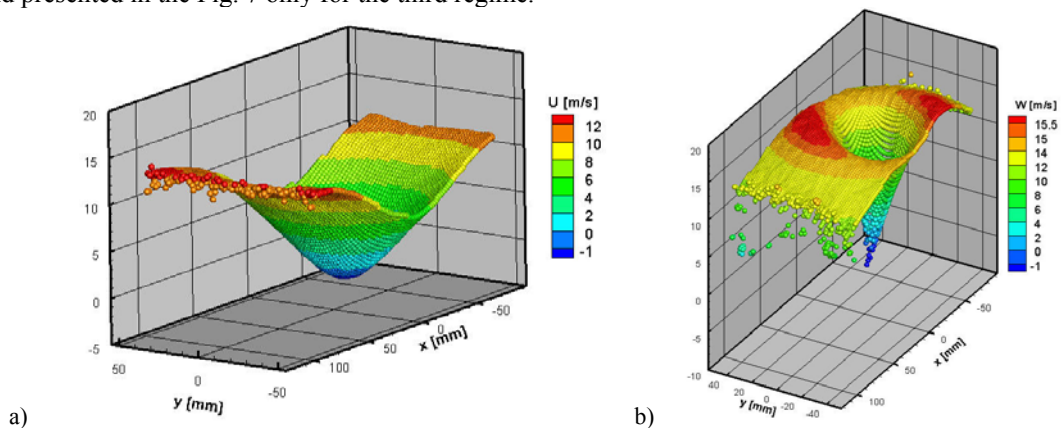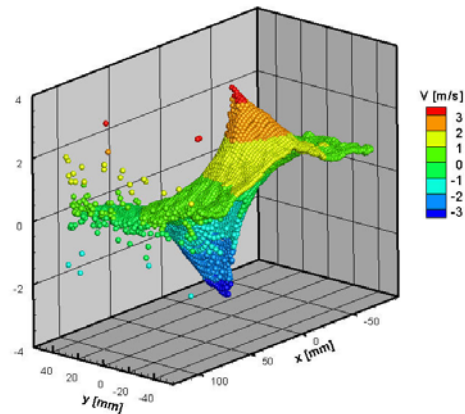
c)
Fig. 7 Velocities for the third regime: a) axial, b) circumferential and c) radial.

Velocity maximums are reached in direction of the x-axis, while in y-axis direction still not. Solid body behaving in vortex core region is visible in Fig. 7b. All maximum values correspond to the adequate measured with LDA (Fig. 3). Cut of the velocity distributions in Fig. 8 with x=x_{cv}, where (x_{cv}, y_{cv}) is vortex core position for the averaged total velocity field, is presented for all five regimes in Fig. 8. It is determined as the position of the minimum of the averaged total velocity field.
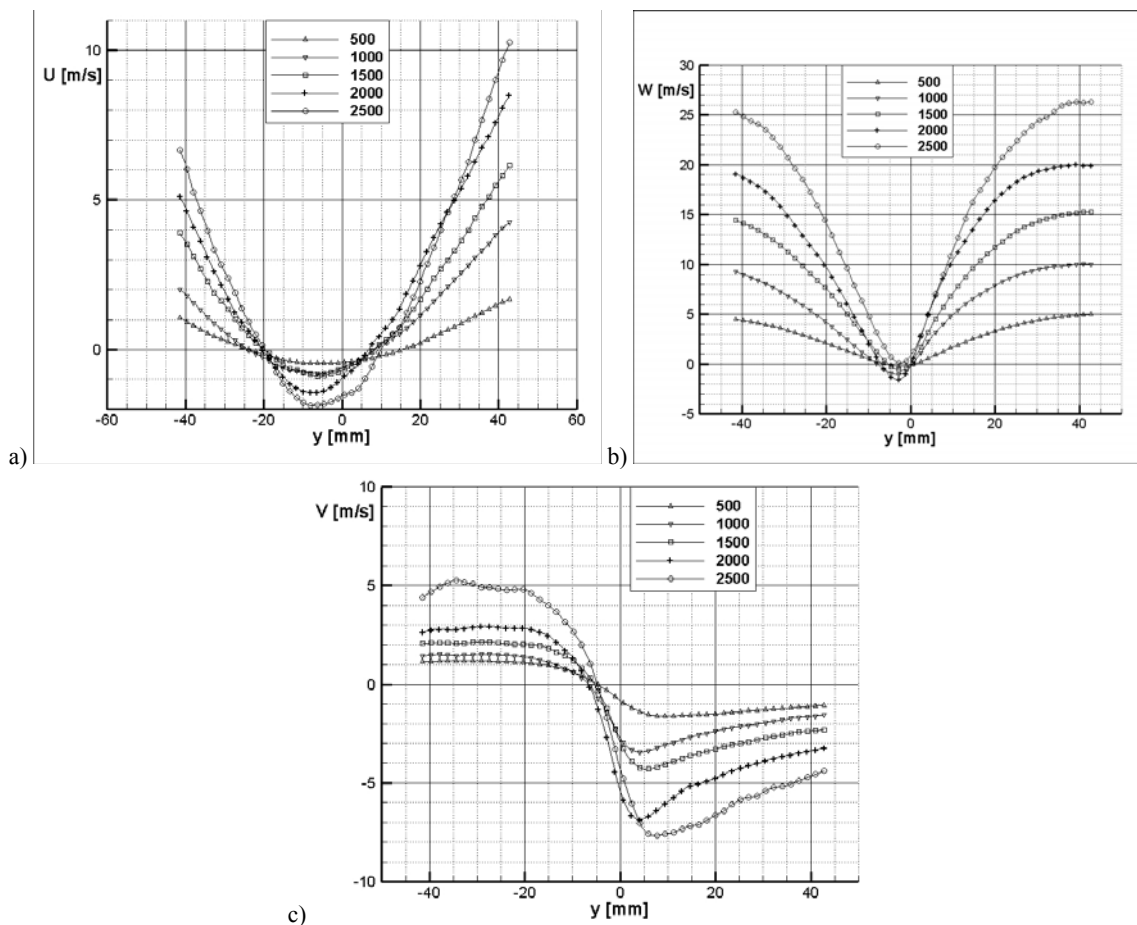

a)

b)

c)

Fig. 8 Velocities distributions for all five regimes: a) axial, b) circumferential and c) radial.

Vortex core off axis is again obvious. Reverse flow is visible and form this angle of view. Negative value of circumferential velocity (Fig. 8b) is a consequence of recalculation of the velocity components to the polar-cylindrical coordinate system with origin in the pipe axis and vortex core off axis position. Radial velocity reached maximum values in the vortex core region.

4.2.2 Dynamics of the vortex core

Positions of the minimum of total velocity fields for 400 pictures is given for the first and the third regime in the following pictures.
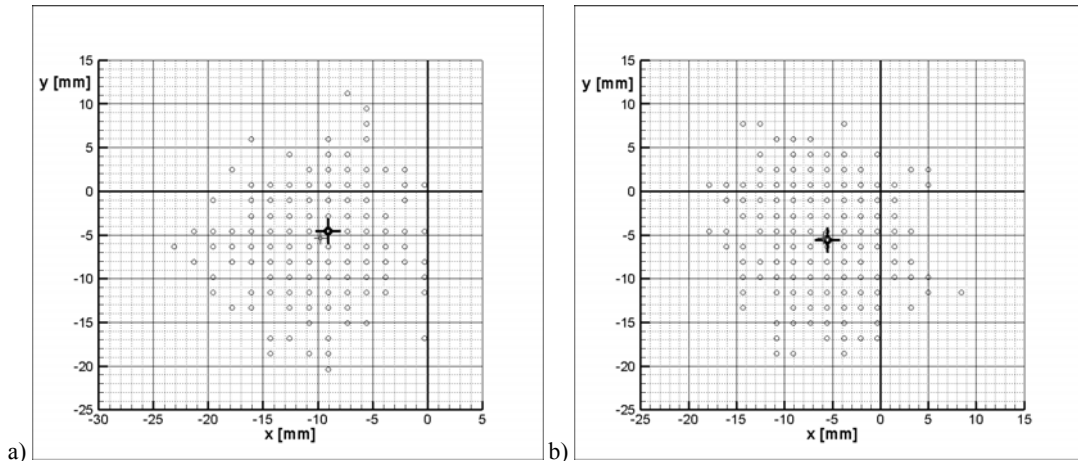

Fig. 9 Total velocity minimum positions for 400 pictures for: a) the first and b) the third regime.

Geometrical centre of all 400 positions is marked with small gray cross, while the minimum of the average total velocity is marked with black one. In the second case, for the third regime, these two crosses almost totally overlap. It is obvious that not all 400 points are visible. It is because some of them are repeated. In the first regime only 10.5% of points are unique, while for the second regime 11.5%. For other three regimes situation is almost the same. Distribution of the repetition number for all regimes is given in the following picture.
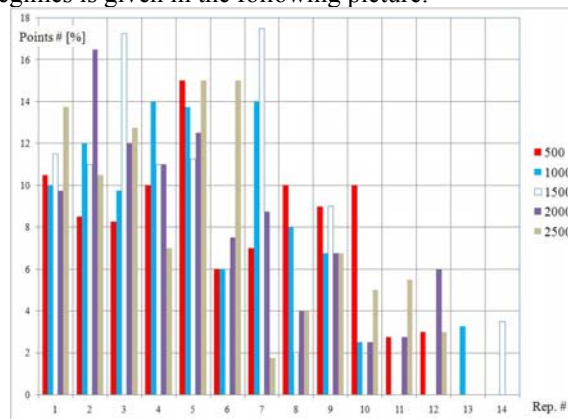

Fig. 10 Number of points vs. repetition number for all five regimes.

Points repetition rate histograms in the (x,y) plane for the first and the third regime are given in the following picture.
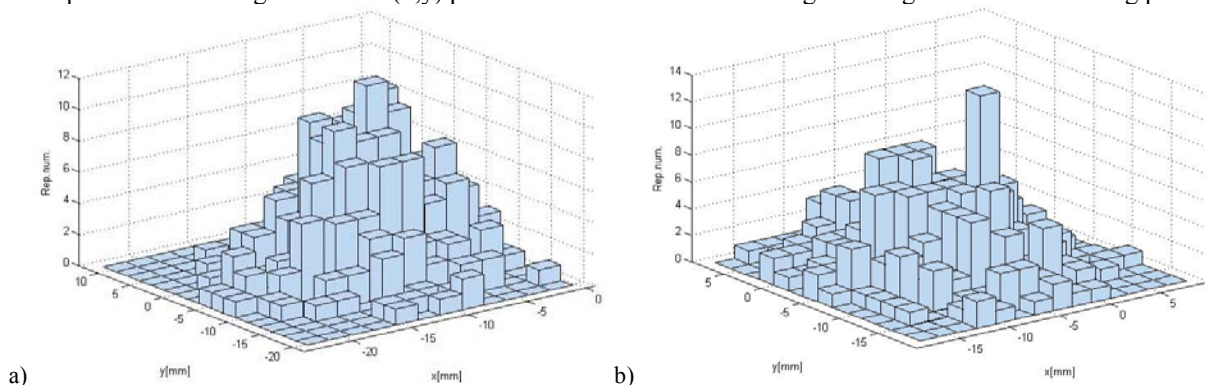

Fig. 11 Points repetition histograms in the (x,y) plane for the a) first and b) third regime.

It can be concluded that repeated points are widely distributed and have different values for higher repetition. These points can be determined. In the following picture are presented vortex center coordinates (Xc,Yc) time dependence for the first and the third regime. These data were taken for 200s.
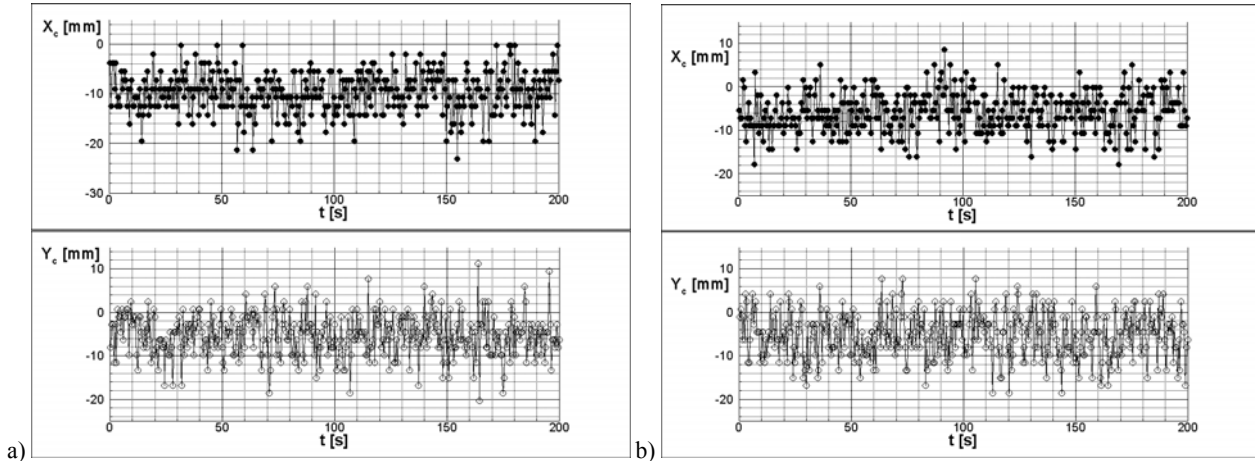

Fig. 12 Vortex core center coordinates for: a) the first and b) the third regime.

From these data (Fig. 12) vortex center coordinates can be determined in each measured time instant. These time distributions show that vortex core location is dominantly in the third quadrant. Also, repetition is visible. However, fan shaft rotation speed is in the interval for all regimes [8.33, 41.67 Hz] and, despite the repetition visibility, these structures must be captured with higher repetition rate.

5. FLUID FLOW VISUALIZATION

Fluid flow visualization has been performed in the section 5 in the pipe cross section and in the meridian plane (Fig. 1).
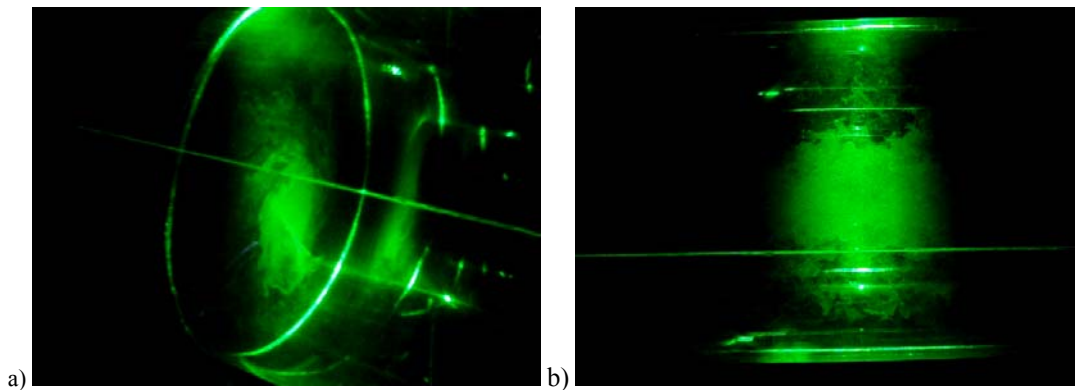

Fig. 13 Fluid flow on the axial fan pressure side in a) corss section and b) vertical meridian plane.

For this reason was employed already mentioned dual Nd:Yag laser with working frequency 15Hz and mounted optics consisted of only one spherical lens with focal length 500mm and one cylindrical lens with f.l. -25mm. Smoke generator (Elven, Precision Limited) probe with Pitot-tube geometry, was positioned upstream the measuring section in position app. *x/D*=17.1. Flow visualization was performed in pipe's cross-section and in meridian section plane. Used camera was SONY, DSC-H3, 10X Optical Zoom, F/3.5-4.4, 8.1MP with max 30 fps. Visualization has proven turbulent swirl flow complexity and vortex core dynamic behavior.

6. CONCLUSION

Complexity of the turbulent swirl flow on the axial fan impeller pressure side has been proven with all applied measuring and visualization techniques. Rankine vortex structure, as fan was designed to produce it, is detected at the axial fan outlet and, it is proven with flow visualization that it is kept till the installation outlet. This fact was also shown in [8]. Vortex core region is smaller downstream, but not significantly. Velocity distributions obtained by use of one component LDA and SPIV show very good agreement. Solid body vortex core structure is shown, as well as

rW=const distribution in the sound flow region. Non-axisymmetry is shown for all five regimes. Turbulence statistics proved non-homogeneity and anisotropy (Fig. 4c) of the investigated flow. Turbulence intensity is great and reaches its maximums for all three velocities in the vortex core region (Fig. 4a and b). Skewness and flatness differ from normal distribution value what is the most dominant in the case of the second and the third regime (Fig. 5). Vortex core dynamics was observed by locating minimum of the total velocity in cross-section. It was shown that number of unique points is approximately the same in the case of all five regimes and is around 10%. Number of points vs. repetition number is given in Fig. 10. Vortex core dynamics was also shown as the dependence $X_c, Y_c = f(t)$. As the bigger frequency is needed for resolving, high speed stereo PIV measurements should be made.

ACKNOWLEDGMENT

References

1. Protić Z.D. et al. *Novel Methods for Axial Fan Impeller Geometry Analysis and Experimental Investigations of the Generated Swirl Turbulent Flow*. Thermal Science 2010, Vol. 14, p. S125

2. Ilić J. et al. *Laser Sheet Scattering and the Cameras' Positions in Particle Image Velocimetry*. Acta Physica Polonica A 2007, Vol. 112, No 5., p. 1113

3. Čantrak S.M. et al. *Problems of Non-Local Turbulent Transfer Modelling*. ZAMM 2001, Vol. 81, S4, p. 913

4. Čantrak Đ.S. et al. *PIV Measurements and Statistical Analysis of the Turbulent Swirl Flow Field. Proc. of ISFV 13 and FLUVISU 12*, Nice, France, 2008

5. Benišek M.H. et al. *Aplication of New Classical Probes in Swirl Fluid Flow Measurements*. Experimental Techniques 2010, Vol. 34, Issue 3, p. 74

6. Čantrak S.M. *Experimentelle Untersuchungen statistischer Eigenschaften turbulenter drallbehafteter Rohr- und Diffusorströmungen*. Dissertation Universität Karlsruhe (TH), Institut für Strömungslehre und Strömungsmaschinen, karlsruhe, 1981

7. Čantrak S.M. et al. *Characteristic Magnitudes Determined from Mean Velocity Distributions of Turbulent Swirling Flow in Pipes*. ZAMM 2001, Vol. 62, Issue 4, p. 201

8. Protić Z.D. et al. *Swirling Flow in the Circular Pipes – the Characteristic Values and Flow-patterns Specifics*. ZAMM 1991, Vol. 71, Issue 5, p. T456

9. Adrian R. *Dynamic Ranges of Velocity and Spatial Resolution of Particle Image Velocimetry*. Meas. Sci. Technol. 1997, Vol. 8, p. 1393.

10. Wereley S. et al. *A Correlation-based Central Difference Image Correction (CDIC) Method and Application in a Four-roll Mill Flow PIV Measurement*. Experiments in Fluids 2003, Vol. 34, p. 42

11. Ramasamy M. et al. *Benchmarking PIV and LDV for Rotor Wake Vortex Flows. 24th Applied Aerodynamics conference Proceedings, AIAA paper 2006-3479,* San Franciso, CA, 2006